

<b>SPIRE</b>	<b>Technical Note</b>	<b>Ref:</b>	SPIRE-RAL-NOT-000993
	Cryostat aperture size requirements including the effects of SPIRE-HERSCHEL misalignments	<b>Issue:</b>	1.00
		<b>Date:</b>	31 October 2001
		<b>Page:</b>	1 of 21

**SUBJECT:**                    **Cryostat aperture size requirements including the effects of SPIRE-HERSCHEL misalignments**

**PREPARED BY:**            **A G Richards**

**KEYWORDS:**                **optical clearance, misalignment, cryostat**

**COMMENTS:**            **This document updates data on the clearance required between SPIRE instrument beams and cryostat apertures. Allowance for the emerging HERSCHEL-SPIRE misalignment budget has been included.**

**DISTRIBUTION:**

B. Swinyard	(RAL)	✓
M Caldwell	(RAL)	✓
A. Richards	(RAL)	
J. Delderfield	(RAL)	✓
K. Dohlen	(LAM)	✓
B. Winter	(MSSL)	✓
M. Griffin	(QMW)	✓
D. DeChambure	(ESTEC)	✓
Project Office	(RAL)	✓

<b>SPIRE</b>	<b>Technical Note</b>	<b>Ref:</b>	SPIRE-RAL-NOT-000993
	<b>Cryostat aperture size requirements including the effects of SPIRE-HERSCHEL misalignments</b>	<b>Issue:</b>	1.00
		<b>Date:</b>	31 October 2001
		<b>Page:</b>	2 of 21

### Contents

1. Introduction .....	2
2. Reference Documents.....	3
3. Optical beam envelopes resumé .....	3
4. Including misalignments into beam clearance calculations .....	5
4.1. Main quantities required.....	5
4.2. Misalignments included and their probability distributions.....	7
4.3. Choosing random tilt and displacement amplitude multiples (N,M) .....	9
4.4. Transforming beam envelopes to allow for tilts and displacements .....	11
4.5. Combining multiple beam envelope extrema into a composite beam envelope. ....	14
5. 3-sigma composite beam boundaries at various locations. ....	14
6. Implications for the SPIRE-HERSCHEL alignment budget.....	19
7. A note on co-ordinate reference frames used.....	20
8. Conclusions and recommendations .....	21

### Figures and Tables

Figure 3-1 Wire-frame representation of a composite photometer beam boundary	4
Figure 3-2 Photometer beam envelope 500-mm forwards of telescope focal surface	4
Figure 3-3 Composite beam boundaries at 771-mm forwards of the telescope axial focus	5
Figure 4-1 Boresight geometry before misalignments	6
Figure 4-2 Boresight geometry after tilts and de-centres applied to SPIRE.	6
Figure 4-3 Distribution of random displacements	7
Figure 4-4 Distribution of random tilts	7
Figure 4-5 Statistics of the computed Photometer RSSQ values for (N,M)=(1,1).	8
Figure 4-6 Photometer pupil alignment budget from RD3	10
Figure 4-7 (N,M) solutions to $RSSQ(N,M,3.0*\sigma,\theta)=11.2$	11
Figure 4-8 Spectrometer beam envelope spreading due to misalignments	12
Figure 4-9 Photometer beam envelope spreading due to misalignments	12
Figure 4-10 Typical statistical spread of beam envelope extrema, Rmaxenv: circles=spectrometer, crosses=photometer	13
Figure 4-11 Statistics of Rmaxenv (circles) for a misaligned spectrometer beam envelope, compared to a normal distribution (crosses)	13
Figure 4-12 Estimated 3-sigma composite beam boundary, 771-mm forward of the axial focus.	14
Figure 5-1 Clearance and 3-sigma composite boundaries at X=523 mm above SPIRE origin.	15
Figure 5-2 Clearance and 3-sigma composite boundaries at X=973 mm above SPIRE origin.	16
Figure 5-3 Clearance and 3-sigma composite boundaries at X=1252 mm above SPIRE origin.	16
Figure 6-1 (N,M) solutions to $RSSQ(N,M,3.0*\sigma,\theta)=9.2$	19
Figure 7-1 Reference co-ordinate systems used.	20
Table 4-1 Main computed quantities defining the instrumental misalignments. ....	5
Table 4-2.....	8
Table 4-3.....	9
Table 4-4 (N,M,θ) solutions to $RSSQ(N,M,3.0*\sigma,\theta)=11.2$ .....	11
Table 4-5 Typical statistics for Rmaxenv for spectrometer and photometer beams .....	13
Table 5-1 (Y,Z) co-ordinates of 90 clearance boundary points in three selected planes .....	17
Table 5-2 (Y,Z) co-ordinates of 90 3-sigma beam boundary points in three selected planes.....	18
Table 6-1 (N,M,θ) solutions to $RSSQ(N,M,3.0*\sigma,\theta)=9.2$ .....	19

<b>SPIRE</b>	<b>Technical Note</b>	<b>Ref:</b>	SPIRE-RAL-NOT-000993
	<b>Cryostat aperture size requirements including the effects of SPIRE-HERSCHEL misalignments</b>	<b>Issue:</b>	1.00
		<b>Date:</b>	31 October 2001
		<b>Page:</b>	3 of 21

## 1. INTRODUCTION

This note updates RD1, which defined the requirements that SPIRE has on the size and shape of the apertures in the thermal shields of the HERSCHEL cryostat and at its entrance port. The new development is the introduction of previously neglected effects due to misalignment of the SPIRE instrument relative to the HERSCHEL telescope and cryostat assembly, prompted by the draft alignment requirements published in RD4.

A model of the misalignment effects using random displacements and tilts within fixed bands, developed in a previous note (RD2), has been utilised to determine overall beam clearance boundaries that are certain (probability > 0.99) to enclose the composite views of both SPIRE instruments, given an upper limit sought for the pupil shear at M2. The upper limits sought for the major contributions to the pupil shear are taken from the SPIRE optical error budget (see RD3).

The details of the derived beam clearance boundaries, which are 10 mm outside the estimated worst-case for the misalignment of SPIRE to HERSCHEL, are given in section 5. The requirement that the space within these clearance boundaries remain clear of warm cryostat and telescope structure imposes a requirement that the cryostat apertures and primary mirror hole be sized accordingly to clear these spaces. The implications that the results have for the HERSCHEL-SPIRE misalignment budget are set out in section 6.

For a note on the two main co-ordinate systems used here, see the section at the end of this note.

## 2. REFERENCE DOCUMENTS

Document	Document number/reference	Document title
RD1	SPIRE-RAL-NOT-000586	SPIRE instrument beam sections forwards of the focal plane aperture plate
RD2	SPIRE-RAL-NOT-000754	Matching SPIRE-HOB Decentre and tilt amplitudes to the photometer pupil alignment budget
RD3	LOOM.KD.SPIRE.2000.002-3	Herschel-SPIRE: Optical error Budgets
RD4	HP-2-ASED-TN-0002	Herschel Alignment Concept

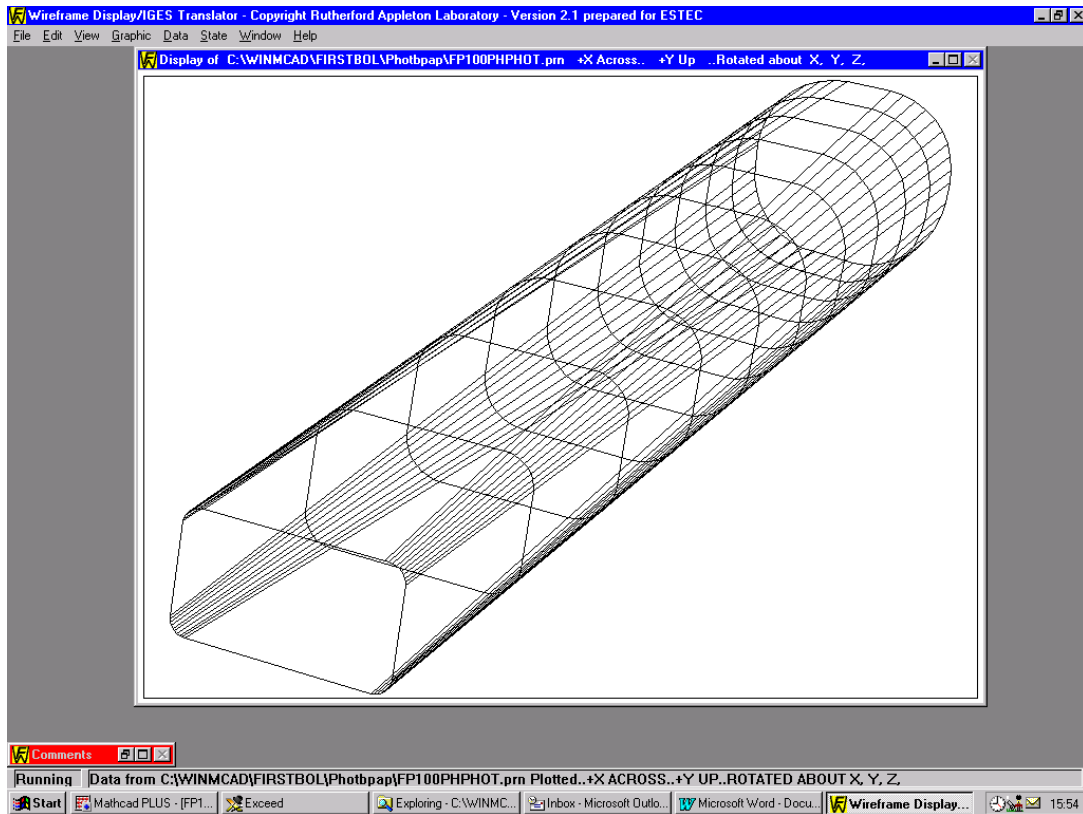
## 3. OPTICAL BEAM ENVELOPES RESUMÉ

Figure 3-1 shows a wireframe model of a section of a geometrical optical beam envelope between two points in the photometer's optical system, namely the telescope focal plane and a plane some distance above it. This structure is defined by two sets of points, one set in the plane at each end of the beam. The envelope is delineated by straight lines joining corresponding points in each set and by cubic spline curves drawn sequentially through the points in each set (see RD1 for more details).

Figure 3-2 shows how the set of points at one end is derived from the boundaries of a set of overlapping beams (sub-pupils) originating from points uniformly spaced around the edge of a detector. A CODEV model of each of the SPIRE instruments was used to generate the rays used to define each sub-pupil beam by tracing from each detector point through points uniformly distributed around the edge of the pupil stop located inside each instrument.

A two-axis steering mirror CM4 is located in the optical path common to both SPIRE instruments. Tilts applied to this mirror are intended to displace the fields of view of both instruments by up to +/- 2 arc minutes on the sky in a direction orthogonal to the fold plane (ESA Y direction) and by about +/- 0.5 arc minutes on the sky parallel to the fold plane (ESA Z direction). Rays were traced through both instruments for the 4 combinations of CM4 tilts that covered the two extremes of each range. A beam envelope was therefore produced for each extreme case and for each instrument, giving 8 beams in total. Figure 3-3 shows a section through such a set of eight beams.

<h1>SPIRE</h1>	<h2>Technical Note</h2>	Ref:	SPIRE-RAL-NOT-000993
	<b>Cryostat aperture size requirements including the effects of SPIRE-HERSCHEL misalignments</b>	Issue:	1.00
		Date:	31 October 2001
		Page:	4 of 21



**Figure 3-1 Wire-frame representation of a composite photometer beam boundary**

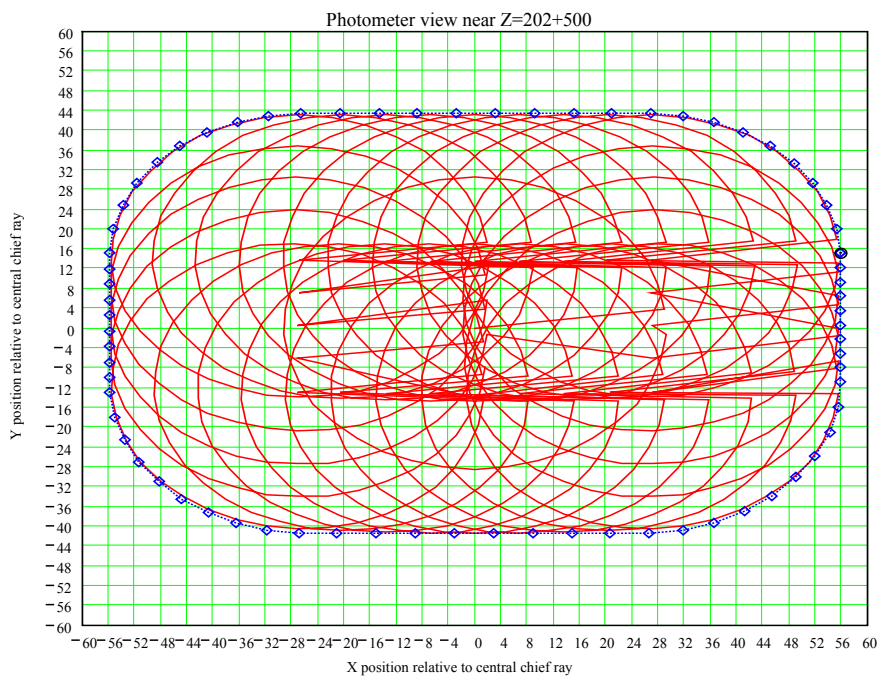


**Figure 3-2 Photometer beam envelope 500-mm forwards of telescope focal surface**

<b>SPIRE</b>	<b>Technical Note</b>	<b>Ref:</b>	SPIRE-RAL-NOT-000993
	Cryostat aperture size requirements including the effects of SPIRE-HERSCHEL misalignments	<b>Issue:</b>	1.00
		<b>Date:</b>	31 October 2001
		<b>Page:</b>	5 of 21

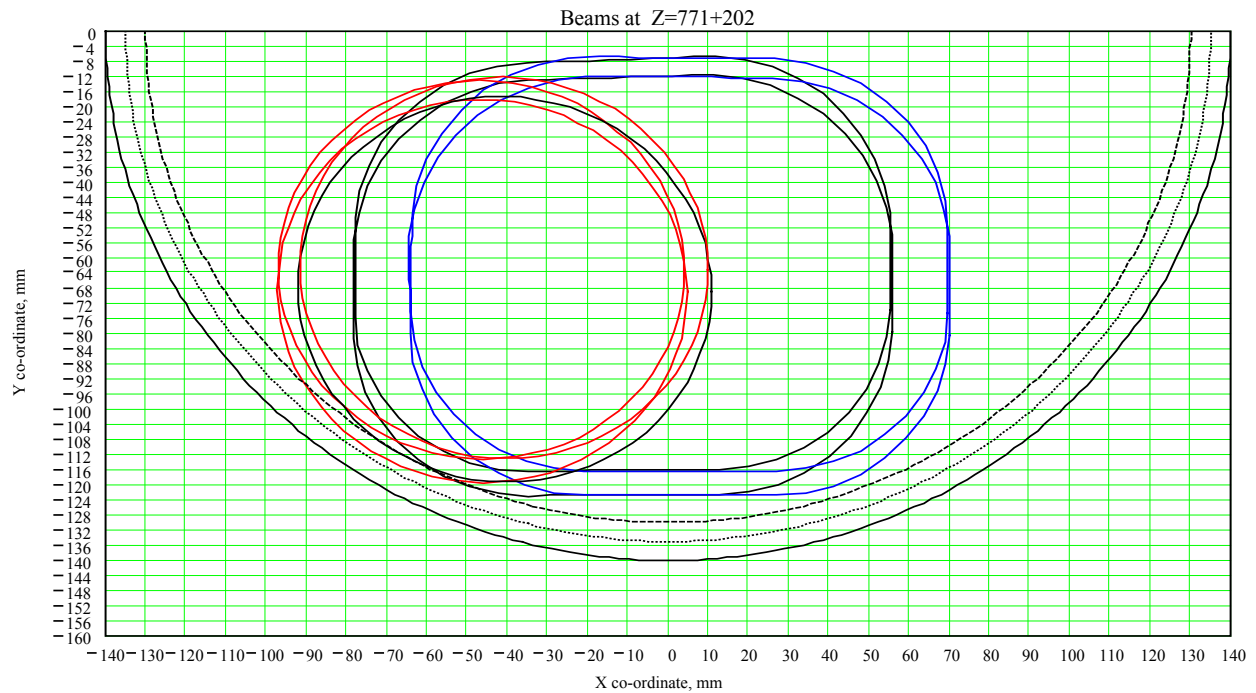


**Figure 3-3 Composite beam boundaries at 771-mm forwards of the telescope axial focus**

The beam boundaries shown in figure 3-3 were obtained by interpolation along beam envelopes such as the one shown in figure 3-1. The location chosen for the particular section shown corresponds to a position near to the front of the cryostat vessel. Superimposed on the figure are sectors of 3 circles, radii 130mm, 135mm and 140mm, each centred on the telescope axis, which can be used as a guide to clearances required at this location. For a note on the two main co-ordinate systems used here, see the section at the end of this note.

#### 4. INCLUDING MISALIGNMENTS INTO BEAM CLEARANCE CALCULATIONS

##### 4.1. Main quantities required.

RD2 describes how the gyrations of SPIRE (and hence its instrument gut rays and optical beams) can be computed, given values for the various co-ordinate displacements and tilts that can be present due to inaccurate placement of each major subsystem (SPIRE, HOB, cryostat, telescope). The essential quantities that are required to define an instrumental misalignment, derived as a function of these individual misalignments, are listed in table 1 and their geometrical relationship shown in figures 4-1 and 4-2 (both taken from RD2).

**Table 4-1 Main computed quantities defining the instrumental misalignments.**

Quantity	Description
$RSSQ(X_{off}, Y_{off}) = \sqrt{X_{off}^2 + Y_{off}^2}$	Lateral displacement of instrument gut ray (boresight vector) from its ideal intersection point at M2
$\Delta X$	Resulting X-shift of the SPIRE instrument relative to its ideal position
$\Delta Y$	Resulting Y-shift of the SPIRE instrument relative to its ideal position
$\Delta Z$	Resulting Z-shift of the SPIRE instrument relative to its ideal position
$\Delta\alpha = \alpha_{new} - \alpha$	Resulting tilt of instrument boresight away from its original direction
$\Delta\beta = \beta_{new} - \beta$	Resulting rotation of instrument fold plane away from its original direction.

<b>SPIRE</b>	<b>Technical Note</b>	Ref:	SPIRE-RAL-NOT-000993
	Cryostat aperture size requirements including the effects of SPIRE-HERSCHEL misalignments	Issue:	1.00
		Date:	31 October 2001
		Page:	6 of 21

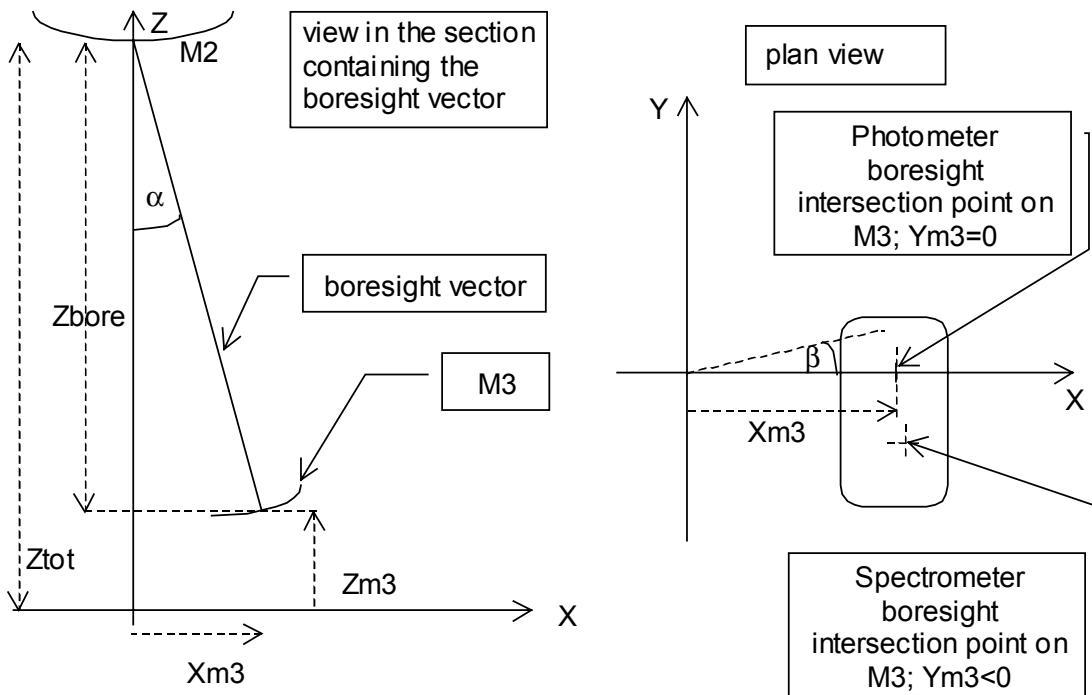


Figure 4-1 Boresight geometry before misalignments

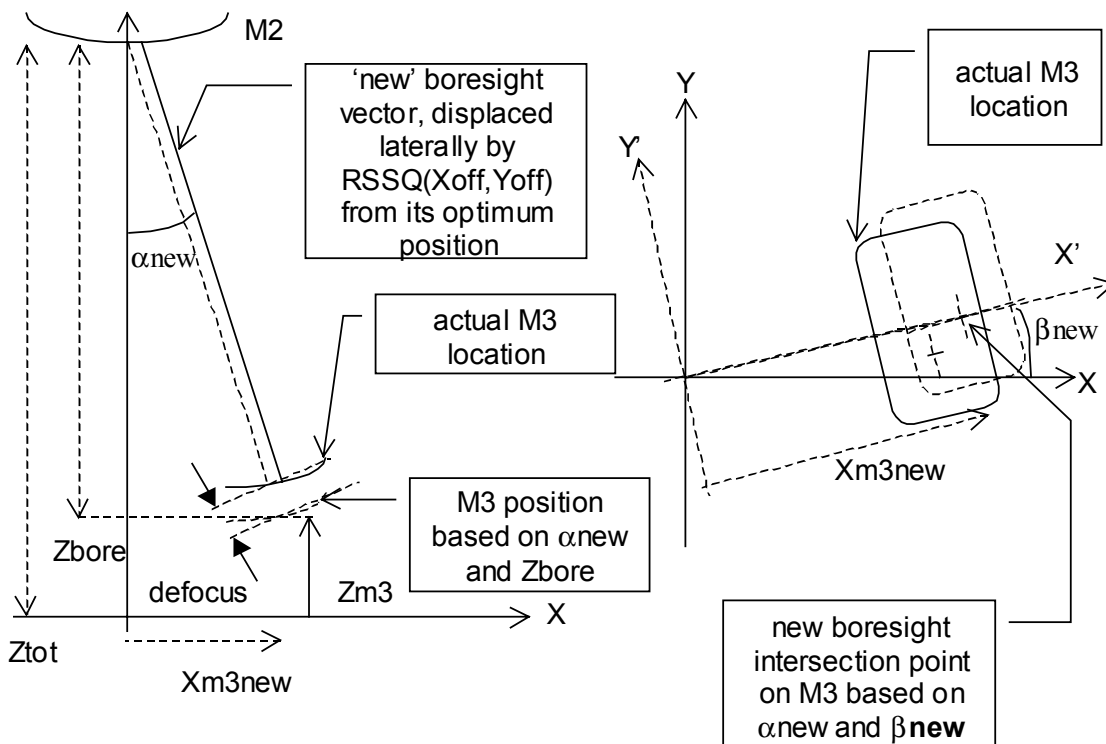
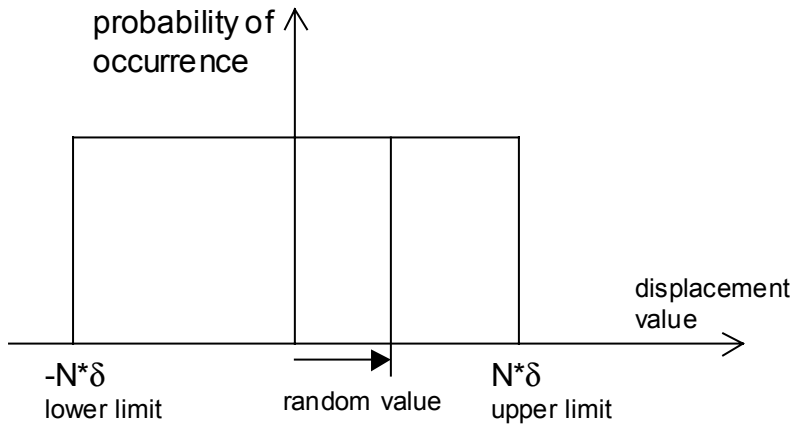


Figure 4-2 Boresight geometry after tilts and de-centres applied to SPIRE.

<b>SPIRE</b>	<b>Technical Note</b>	<b>Ref:</b>	SPIRE-RAL-NOT-000993
	Cryostat aperture size requirements including the effects of SPIRE-HERSCHEL misalignments	<b>Issue:</b>	1.00
		<b>Date:</b>	31 October 2001
		<b>Page:</b>	7 of 21

#### 4.2. Misalignments included and their probability distributions

RD2 lists the 6 displacements and 6 tilts included in the misalignment model. For the Monte Carlo computations, each displacement was taken to be a random quantity uniformly selected from within a fixed range of values extending from  $-N*\delta$  to  $+N*\delta$ , with  $\delta=0.5$  mm., as illustrated in figure 4-3. Each tilt was taken to be a random quantity uniformly selected from within a fixed range of values extending from  $-M*q$  to  $+M*q$ , with  $q=1$  arc minute = 0.0003 radians, as illustrated in figure 4-4.



**Figure 4-3 Distribution of random displacements**

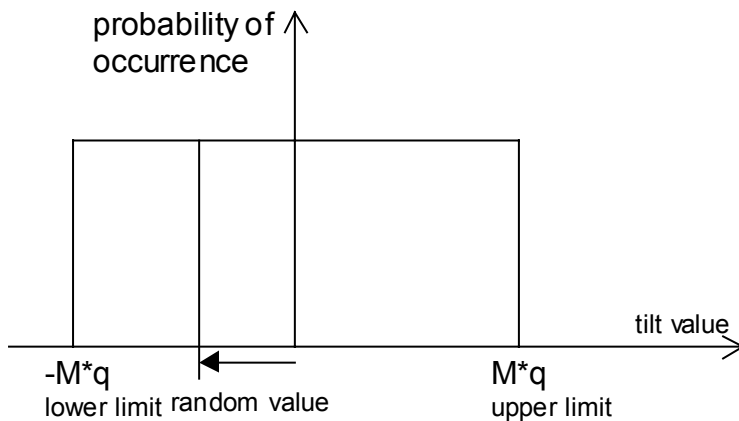


**Figure 4-4 Distribution of random tilts**

The main quantities determining the sizes of the random displacements and tilts were therefore the values that had to be chosen for the parameters  $N$  and  $M$ , the multiples of the unit displacements and tilts defining the allowed ranges of each random variable. This choice was aided by the following relationship discovered in RD2 between the distribution of  $RSSQ(Xoff, Yoff)$ , the resulting random values for the lateral boresight offset from the centre of M2, and the number pairs  $(N,M)$ :

<b>SPIRE</b>	<b>Technical Note</b>	Ref:	SPIRE-RAL-NOT-000993
	Cryostat aperture size requirements including the effects of SPIRE-HERSCHEL misalignments	Issue:	1.00
		Date:	31 October 2001
		Page:	8 of 21

$$RSSQ(M, N, f * \sigma, \theta) = \sqrt{N^2 + M^2} * \{A1(f) + A2(f) * \cos(2\theta - A3(f))\} \quad (4-1)$$

$$\theta(M, N) = \tan^{-1}\{N/M\} \quad (4-2)$$

In equation (4-1),  $f$  represents the multiple of the standard deviation  $\sigma$  of the distribution away from the mean value that the RSSQ value represents, as shown in figure 4-5, which shows some results of computing  $RSSQ(X_{off}, Y_{off})$  for 1000 random sets of values for the displacements and tilts with  $(N, M) = (1, 1)$ . The distribution of RSSQ (circles) is compared with a normal distribution (crosses) having the same mean and standard deviation, proving that it is close to a normal distribution.

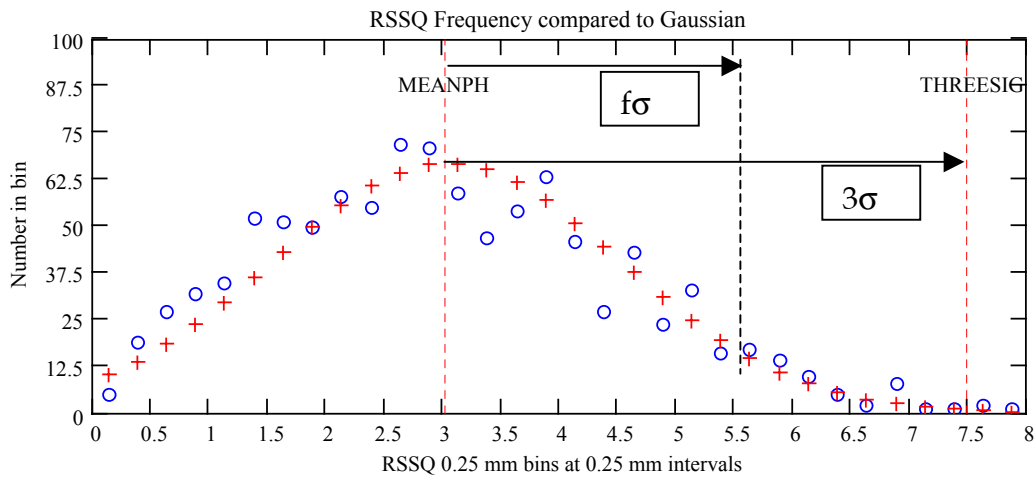


**Figure 4-5 Statistics of the computed Photometer RSSQ values for  $(N, M) = (1, 1)$ .**

Table 4-2 shows some values computed for the coefficients  $A1$ ,  $A2$  and  $A3$  in equation (4-1) for some values chosen for the parameter  $f$ . Also shown are the values for the mean, mean+ $3\sigma$  values and the maximum value of  $RSSQ(X_{off}, Y_{off})$  actually found for the distribution given by the choice  $(N, M) = (1, 1)$ .

**Table 4-2**

	A1	A2	A3 (degrees)
$f=1.0$	1.005	0.245	8
$f=1.28$	1.105	0.265	8
$f=3.0$	1.655	0.395	11
(N,M)	Mean RSSQ	Mean+ $3\sigma$	Max RSSQ
(1,1)	3.025	7.503	7.99

The distribution of RSSQ values shown in figure 4-5, although closely following a normal distribution, differs from that type of distribution in one important respect: there is a maximum value for RSSQ that can occur. This follows from the restrictions, shown in figures 4-3 and 4-4, on the absolute magnitudes of the 12 random variables whose deviations from zero contribute to the

<b>SPIRE</b>	<b>Technical Note</b>	<b>Ref:</b>	SPIRE-RAL-NOT-000993
	<b>Cryostat aperture size requirements including the effects of SPIRE-HERSCHEL misalignments</b>	<b>Issue:</b>	1.00
		<b>Date:</b>	31 October 2001
		<b>Page:</b>	9 of 21

values finally achieved for RSSQ(Xoff,Yoff). In table 4-2 we show the maximum value reached by RSSQ(Xoff,Yoff) for a particular combination of (N,M)=(1,1) was 7.99. The value of (mean+3\*σ)=7.5 for this particular distribution. In fact it was found that for all combinations of (N,M) tried, the maximum value achieved in 1000 determinations of RSSQ(Xoff,Yoff) was always close to the value of (mean+3\*σ) for the distribution of values for RSSQ(Xoff,Yoff).

Given a normal distribution for any random quantity, table 4-3 shows the cumulative probabilities for obtaining a value less than the quoted value by random selection:

**Table 4-3**

Upper limit	Probability that a value less than this upper limit will be obtained by random selection
Mean of normal distribution	0.5
Mean + σ	0.841
Mean + 1.28σ	0.9
Mean + 3σ	0.9987

### 4.3. Choosing random tilt and displacement amplitude multiples (N,M)

If we choose to select an upper limit for RSSQ(Xoff,Yoff) = mean + 3σ, then this requires us to choose (N,M) such that equation (4-1), with coefficients (A1(f),A2(f),A3(f)) taken from the **f=3** case in table (4-2), gives this value. With (N,M) so chosen, we can then be almost certain (probability >0.99) that no randomly-generated value for RSSQ(Xoff,Yoff) will exceed this upper limit.

We start by selecting a ‘3-sigma’ target value for RSSQ(Xoff,Yoff). This is done by considering the values presently assigned to the three main contributions to the overall ‘pupil alignment’ budget for the photometer and spectrometer. These are given in the tree shown in figure 4-6, which has been reproduced from RD3. In this tree, the three major contributors are shown in boxes with thick outlines. In RD1, the delineation of the space required to be kept clear of structure as the SPIRE optical beams traverse the cryostat space contains an allowance for the component named as ‘Design(pupil aberrations)’. This is because the photometer and spectrometer beam envelopes are sized to cover the actual geometrical optical full field of view of each instrument and so they include the pupil aberrations that vary with field angle. This component of the alignment budget is deterministic, rather than statistical, in that it is fixed by the distortions inherent in the slightly imperfect imagery that each optical system is forced by trade-offs to produce (even when perfectly aligned). However, no allowance was made in RD1 for the other two major sources of misalignment, namely SPIRE-to-HOB misalignment and internal misalignments in each of the SPIRE instruments. Since they are subject to random effects, these two components are shown root-sum-squared together to give the overall ‘Alignment’ contribution which is shown equivalent to a 11.2 mm pupil shear at M2.

<b>SPIRE</b>	<b>Technical Note</b>		<b>Ref:</b>	SPIRE-RAL-NOT-000993
	Cryostat aperture size requirements including the effects of SPIRE-HERSCHEL misalignments		<b>Issue:</b>	1.00
			<b>Date:</b>	31 October 2001
			<b>Page:</b>	10 of 21

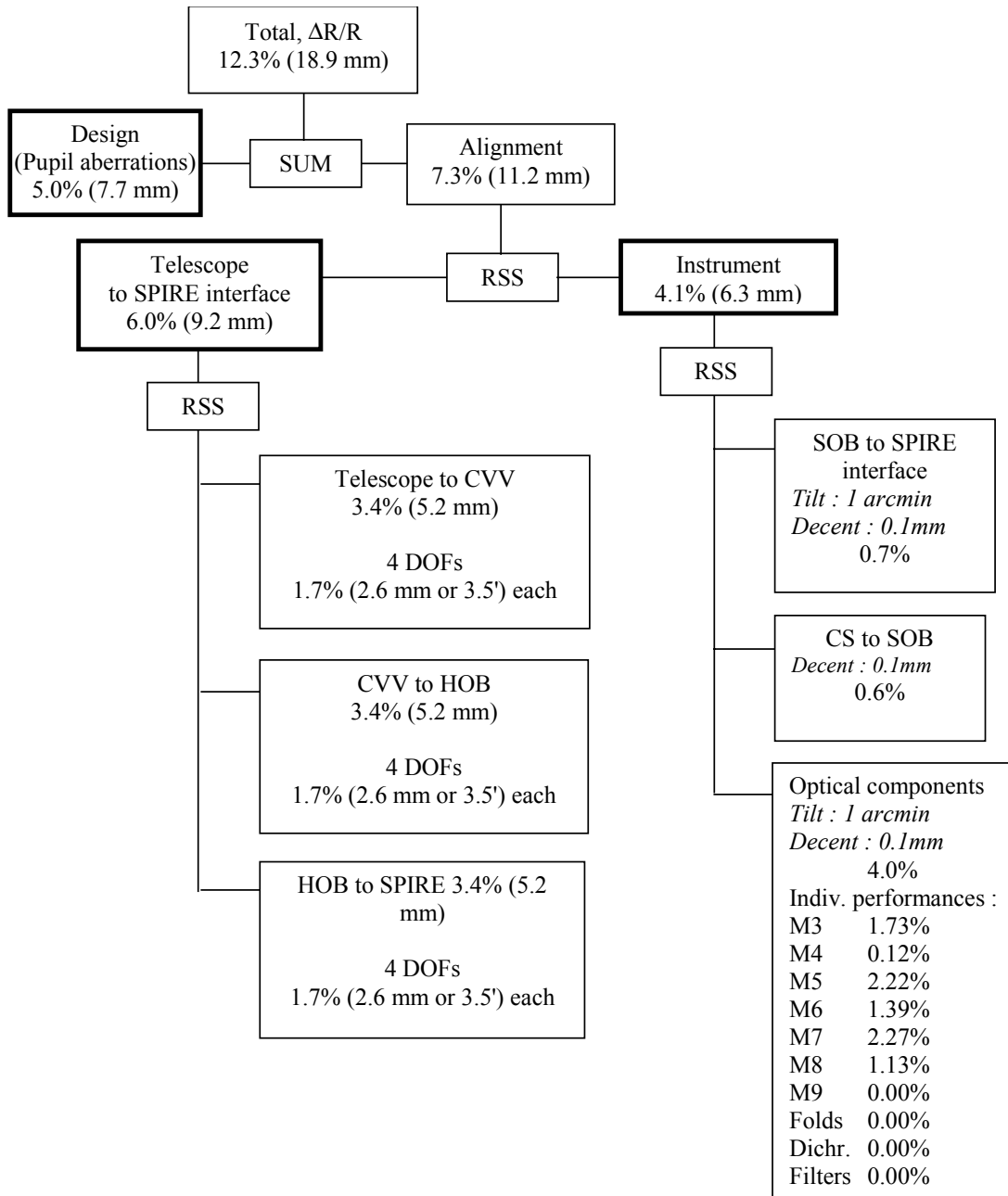


**Figure 4-6 Photometer pupil alignment budget from RD3**

It therefore makes sense to select the value 11.2 mm as our ‘mean + 3σ’ value for the RSSQ(Xoff,Yoff) distribution that we seek. Based on this choice, solution of the inverse of equation (4-1) to find the pairs (N,M) that will produce RSSQ(Xoff,Yoff,3\*σ)=11.2 mm was carried out with the results graphed in figure 4-7 and listed in table 4-4.

<b>SPIRE</b>	<b>Technical Note</b>	<b>Ref:</b>	SPIRE-RAL-NOT-000993
	<b>Cryostat aperture size requirements including the effects of SPIRE-HERSCHEL misalignments</b>	<b>Issue:</b>	1.00
		<b>Date:</b>	31 October 2001
		<b>Page:</b>	11 of 21

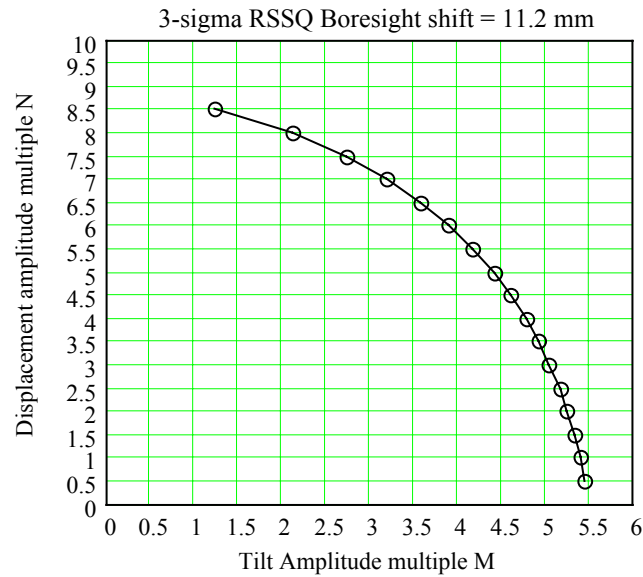


**Figure 4-7 (N,M) solutions to  $RSSQ(N,M,3.0*\sigma,\theta)=11.2$**

N	M	$\theta$
0.5	5.442	5.25
1	5.387	10.52
1.5	5.323	15.74
2	5.247	20.87
2.5	5.157	25.86
3	5.041	30.76
3.5	4.922	35.42
4	4.777	39.94
4.5	4.606	44.33
5	4.405	48.62
5.5	4.172	52.82
6	3.894	57.02
6.5	3.569	61.23
7	3.183	65.55
7.5	2.716	70.09
8	2.101	75.29
8.5	1.224	81.81

**Table 4-4 (N,M, $\theta$ ) solutions to  $RSSQ(N,M,3.0*\sigma,\theta)=11.2$**

The curve in figure 4-7 allows us to select any pair of (N,M) values which together will ensure a distribution of  $RSSQ(X_{off},Y_{off})$  values which will be 99% certain to be less than 11.2 mm. In the first instance, a choice was made for (N,M)=(6,3.89), yielding limits for the random displacement errors = (+3  $\rightarrow$  - 3 mm) and limits for the random tilt errors = (-3.89 arc minutes  $\rightarrow$  +3.89 arc minutes). These limits were then imposed on the 12 random variables that are used, as described in RD2, to generate 1000 random values for the instrumental boresight shifts and tilts listed in table 4-1. These 1000 shifts and tilts were then applied to the instrument beam envelopes in the manner shown in the next section.

#### 4.4. Transforming beam envelopes to allow for tilts and displacements

Each point (X<sub>env</sub>,Y<sub>env</sub>,Z<sub>env</sub>) that contributes to the definition of a beam envelope for a perfectly aligned SPIRE-HERSCHEL system must be transformed to allow for the fact that SPIRE is tilted and shifted by the quantities listed in table 4-1. This is done using the following transformation:

<b>SPIRE</b>	<b>Technical Note</b>	Ref:	SPIRE-RAL-NOT-000993
	Cryostat aperture size requirements including the effects of SPIRE-HERSCHEL misalignments	Issue:	1.00
		Date:	31 October 2001
		Page:	12 of 21

$$\begin{pmatrix} X'_{env} \\ Y'_{env} \\ Z'_{env} \end{pmatrix} = \begin{pmatrix} \cos(\beta - \beta_{new}) & \sin(\beta - \beta_{new}) & 0 \\ -\sin(\beta - \beta_{new}) & \cos(\beta - \beta_{new}) & 0 \\ 0 & 0 & 1 \end{pmatrix} \begin{pmatrix} \cos(\alpha - \alpha_{new}) & 0 & -\sin(\alpha - \alpha_{new}) \\ 0 & 1 & 0 \\ \sin(\alpha - \alpha_{new}) & 0 & \cos(\alpha - \alpha_{new}) \end{pmatrix} \begin{pmatrix} X_{env} \\ Y_{env} \\ Z_{env} \end{pmatrix} + \begin{pmatrix} \Delta X \\ \Delta Y \\ \Delta Z \end{pmatrix}$$

Once the co-ordinates of all points defining the start and end of a beam envelope have been transformed in this way, then the intersection of the transformed beam envelope with a particular plane located along the telescope axis can be computed and plotted out. Note that all 8 beam envelopes are transformed simultaneously, using the SAME set of tilt angles and shifts. When this is done 1000 times, covering the set of random alignments, the overlap of the transformed sections gives an idea of the maximum spread likely due to misalignments that give  $RSSQ(X_{off}, Y_{off}) < 11.2$  mm. Figure 4-8 shows a spectrometer beam section after adding random misalignments and figure 4-9 shows a photometer beam section. Both beams were selected from figure 3-3 as the ones with initial boundaries that came nearest to the edge of the 140-mm circle plotted on each figure.

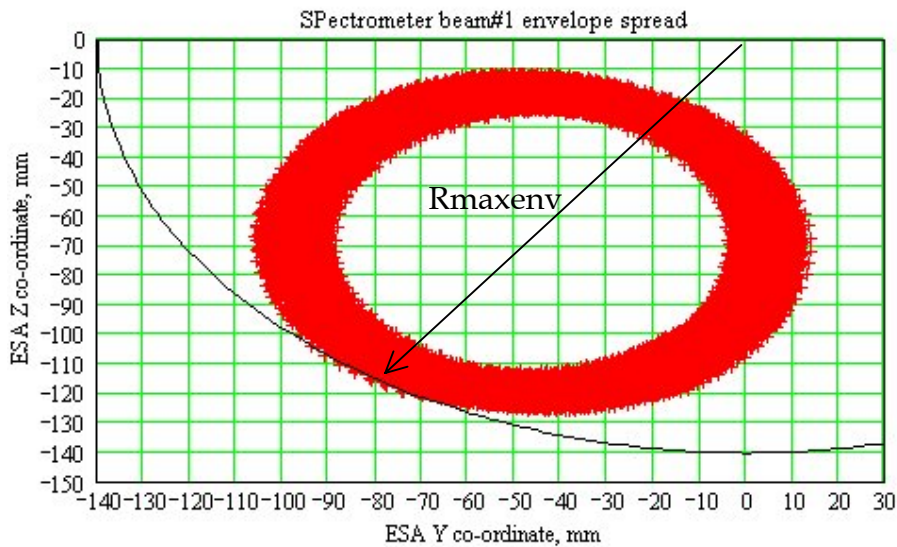


Figure 4-8 Spectrometer beam envelope spreading due to misalignments

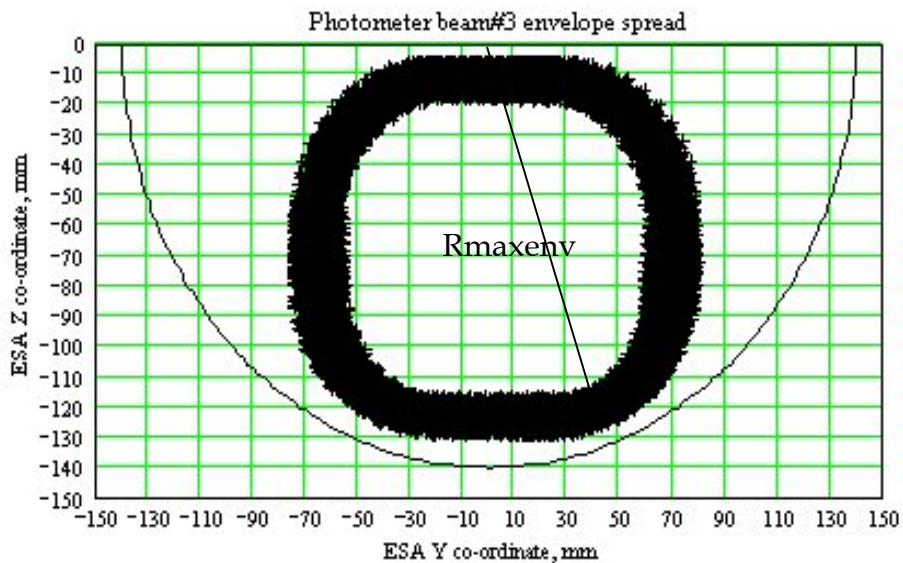
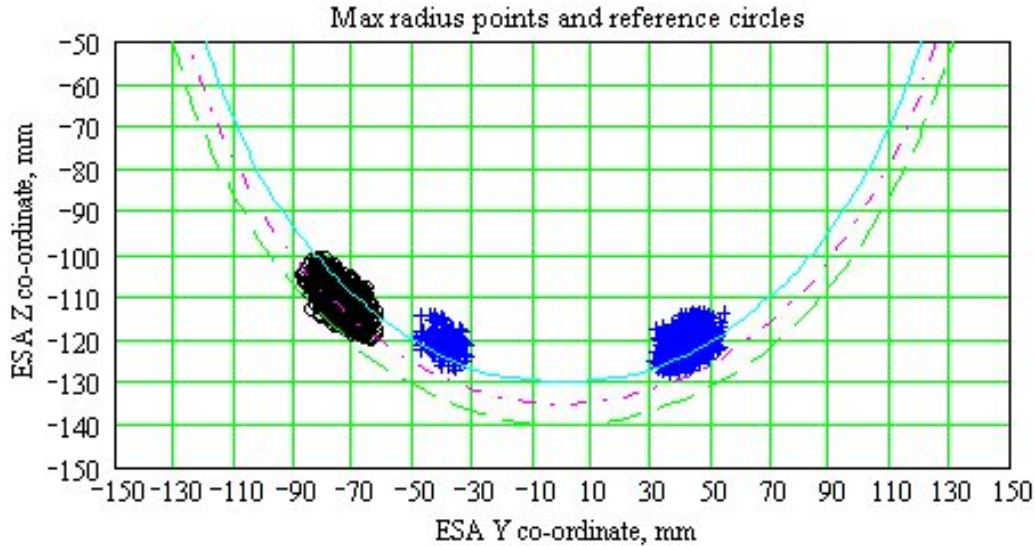


Figure 4-9 Photometer beam envelope spreading due to misalignments

<b>SPIRE</b>	<b>Technical Note</b>	Ref:	SPIRE-RAL-NOT-000993
	Cryostat aperture size requirements including the effects of SPIRE-HERSCHEL misalignments	Issue:	1.00
		Date:	31 October 2001
		Page:	13 of 21

It is interesting to examine the statistics of Rmaxenv, the maximum distance from the telescope axis reached by each misaligned beam envelope (indicated on the figures). These data are plotted in figure 4-10 for the two beam envelopes selected from figure 3-3 for illustration. Statistical data are collected in table 4-5. Figure 4-11 shows that Rmaxenv follows very closely a normal distribution.



**Figure 4-10 Typical statistical spread of beam envelope extrema, Rmaxenv: circles=spectrometer, crosses=photometer**

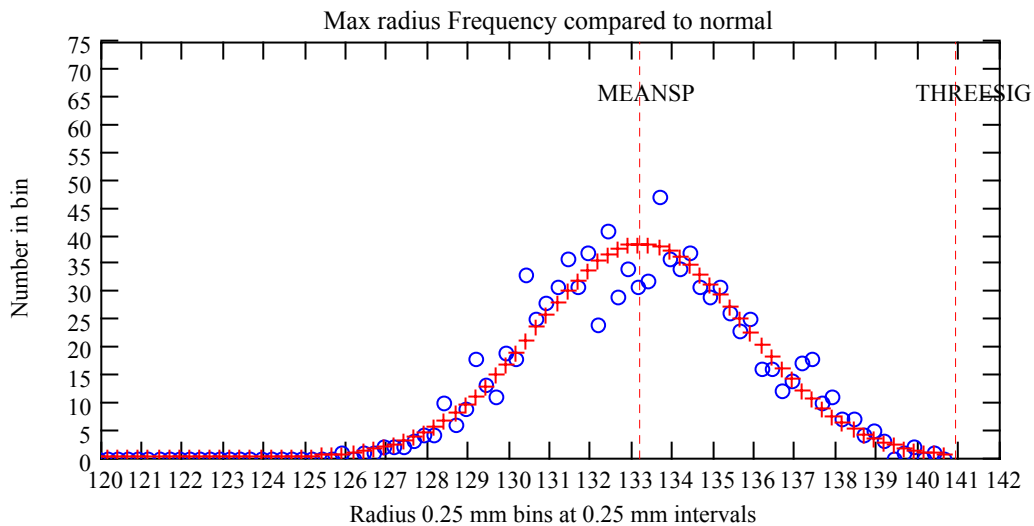


**Figure 4-11 Statistics of Rmaxenv (circles) for a misaligned spectrometer beam envelope, compared to a normal distribution (crosses)**

**Table 4-5 Typical statistics for Rmaxenv for spectrometer and photometer beams**

beam	Mean value	Rmaxenv statistics	
		Mean+3*sigma	Maximum value found
Spectrometer	133.20	140.96	140.958
Photometer	127.31	134.88	133.82

<b>SPIRE</b>	<b>Technical Note</b>	Ref:	SPIRE-RAL-NOT-000993
	Cryostat aperture size requirements including the effects of SPIRE-HERSCHEL misalignments	Issue:	1.00
		Date:	31 October 2001
		Page:	14 of 21

Table 4-5 shows that the maximum value reached when computing  $R_{maxenv}$  for a given beam is quite close to the value of  $(mean+3*\sigma)$  for the distribution of the same quantity. This is as expected, based on the earlier results of computations of the tilts and displacements that are used to transform the beam envelopes to their misaligned locations.

#### 4.5. Combining multiple beam envelope extrema into a composite beam envelope.

Figures 4-8 and 4-9 show the spread of 1000 beam envelopes after randomly-generated tilt and displacement misalignments have been applied. They cover just two of the eight geometrical optical beams shown in figure 3-3 that must be included. By combining these data with similar data for the remaining 6 beams, a complete composite beam envelope can be constructed. The result is a figure such as 3-3 but with each envelope broadened by the spread imposed by 1000 random misalignments. The outermost boundary of this complete composite beam envelope is what is wanted. Figure 4-12 shows such a beam envelope, computed in the same plane as is displayed in figure 3-3. The ‘wobble’ on the boundary curve reflects statistical sampling noise combined with the finite resolution imposed by the spacing between the points used to define each beam envelope. Based on the statistical analysis described here, we can be 99% confident that, in this plane, the combined envelope of the spectrometer and photometer geometrical optical views will not go beyond the smooth curve drawn through the outermost points on this boundary, provided that the 12 random displacement and tilt misalignments remain within their specified limits. For shorthand purposes, this envelope will hereafter be referred to as a ‘3-sigma composite beam boundary’.

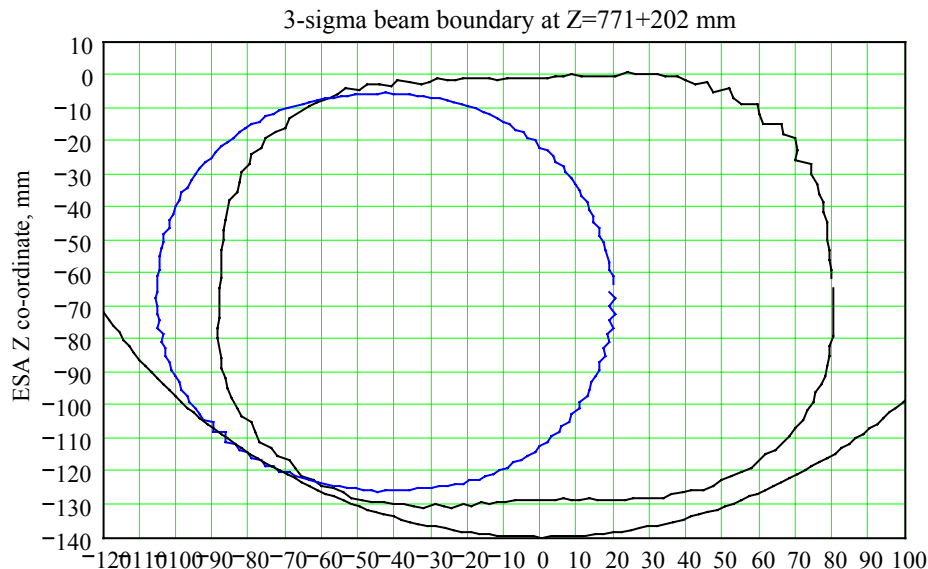


**Figure 4-12 Estimated 3-sigma composite beam boundary, 771-mm forward of the axial focus.**

For practical purposes, it is necessary to smooth out the ripples in the boundary curve shown in figure 4-12 by selecting points on the boundaries which, when joined up, define a boundary that completely encloses the figure. Then we can add a ‘clearance’ border around it, so that we can define an aperture that should clear the 3-sigma beam by the minimum desired amount in the worst case of a 3-sigma occurrence of a beam deviation from its mean location.

#### 5. 3-SIGMA COMPOSITE BEAM BOUNDARIES AT VARIOUS LOCATIONS.

In this section we detail the shape of the 3-sigma composite beam boundaries at three locations. These are at 321-mm above the telescope axial focus, at 771-mm above the focus and at 1050-mm

<b>SPIRE</b>	<b>Technical Note</b>	Ref:	SPIRE-RAL-NOT-000993
	Cryostat aperture size requirements including the effects of SPIRE-HERSCHEL misalignments	Issue:	1.00
		Date:	31 October 2001
		Page:	15 of 21

above the focus. The latter figure puts the beam section level with the pole of the primary mirror and hence can be compared with the size of the hole in the primary mirror. In what follows we use the ESA co-ordinate system (see section 7), which aligns +X along the telescope axis, +Z towards the sunshade (pointing away from SPIRE). The co-ordinate origin used by SPIRE is located 202 mm behind the axial focus, so the selected planes are at  $X=321+202$ ,  $X=771+202$  and  $X=1050+202$  in this system.

Each clearance beam boundary associated with a 3-sigma boundary is formed by adding a 10-mm wide clearance border around the 3-sigma composite beam boundary. The 10 millimetres are added approximately along the local normal to the 3-sigma boundary curve. The pairs of clearance and 3-sigma boundaries are shown in figures 5-1, 5-2 and 5-3. Each curve is made up of 90 points, each arc length drawn between pairs of points subtending 4 degrees at the mean centre of the set of points. The co-ordinates of each point are given in tables 5-1 (clearance boundary), and 5-2 (3-sigma composite boundary). Approximate clearance curves for planes located at other values of X can be obtained by linear interpolation between the data given for the planes at  $X=523$ ,  $X=973$  and  $X=1252$ .

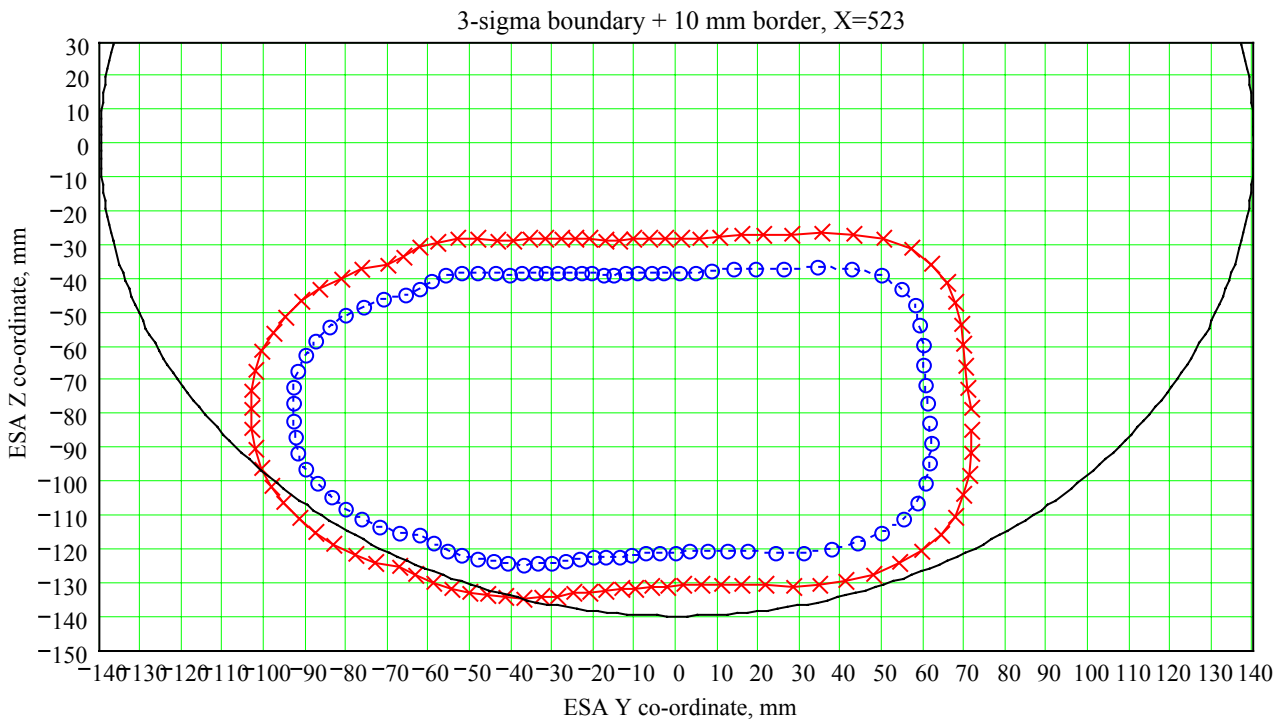


**Figure 5-1 Clearance and 3-sigma composite boundaries at X=523 mm above SPIRE origin.**

<b>SPIRE</b>	<b>Technical Note</b>	Ref:	SPIRE-RAL-NOT-000993
	Cryostat aperture size requirements including the effects of SPIRE-HERSCHEL misalignments	Issue:	1.00
		Date:	31 October 2001
		Page:	16 of 21

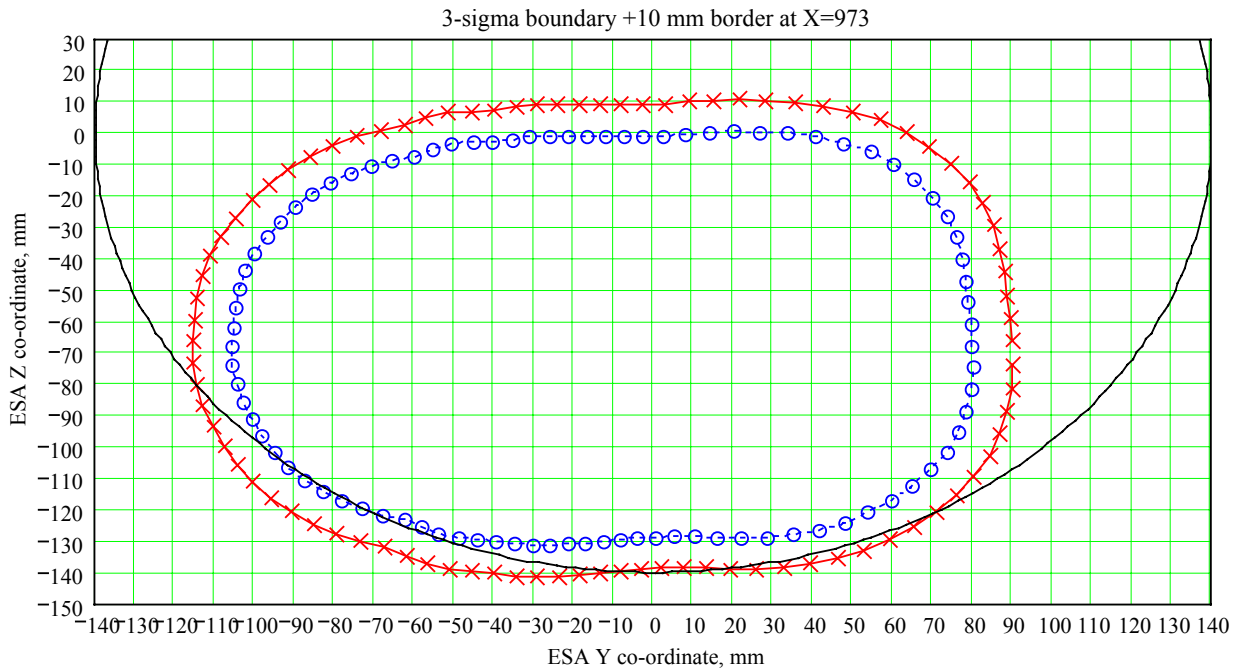


**Figure 5-2 Clearance and 3-sigma composite boundaries at X=973 mm above SPIRE origin.**

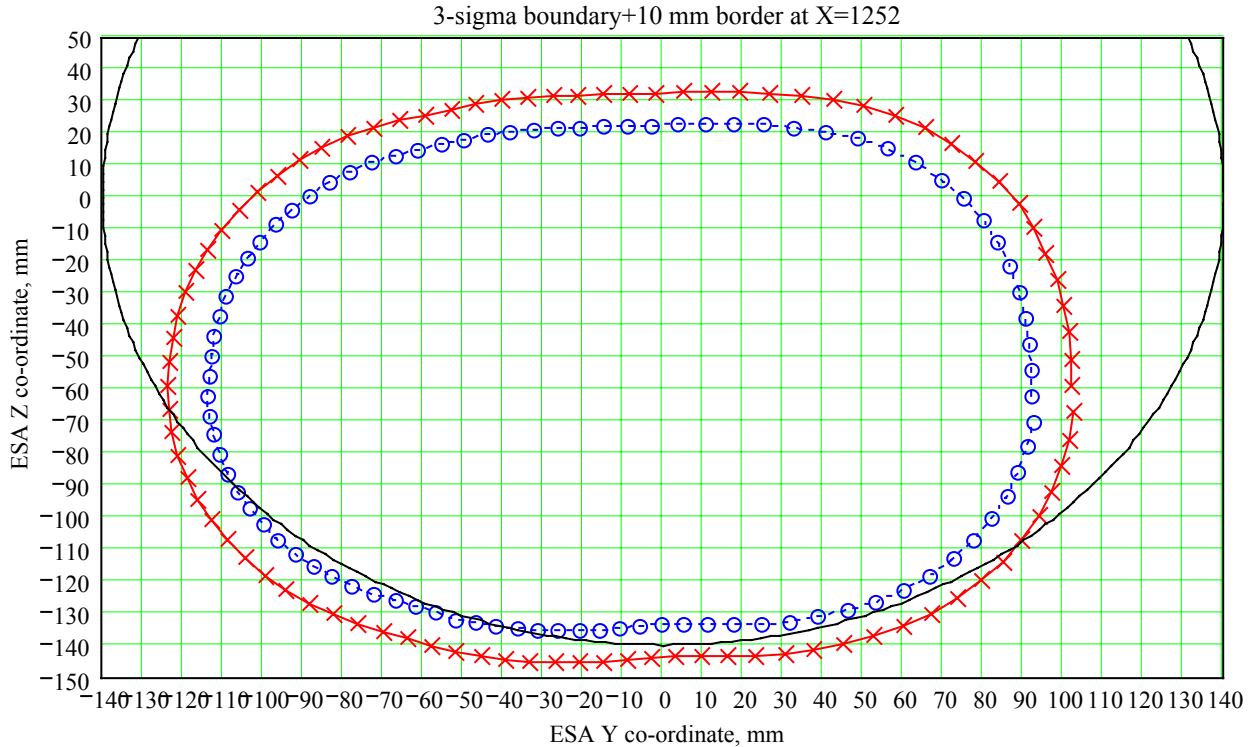


**Figure 5-3 Clearance and 3-sigma composite boundaries at X=1252 mm above SPIRE origin.**

<b>SPIRE</b>	<b>Technical Note</b>						Ref:	SPIRE-RAL-NOT-000993
	Cryostat aperture size requirements including the effects of SPIRE-HERSCHEL misalignments						Issue:	1.00
							Date:	31 October 2001
							Page:	17 of 21

**Table 5-1 (Y,Z) co-ordinates of 90 clearance boundary points in three selected planes**

	X = 523		X = 973		X = 1252				X = 523		X = 973		X = 1252	
point	Y ESA	Z ESA	Y ESA	Z ESA	Y ESA	Z ESA		point	Y ESA	Z ESA	Y ESA	Z ESA	Y ESA	Z ESA
1	71.3	-78.9	89.7	-66.5	102.0	-59.0		46	-103.3	-78.9	-115.7	-66.5	-123.6	-59.0
2	70.4	-72.6	89.3	-59.1	101.7	-50.6		47	-103.2	-84.8	-115.6	-73.4	-123.3	-66.4
3	69.9	-66.4	88.7	-51.7	101.2	-42.3		48	-102.5	-90.6	-114.7	-80.3	-122.5	-73.7
4	69.6	-60.0	88.1	-44.3	100.1	-33.9		49	-101.1	-96.3	-113.0	-87.1	-121.1	-80.9
5	68.7	-53.6	86.8	-37.0	98.2	-25.7		50	-98.7	-101.6	-110.6	-93.6	-119.0	-87.9
6	67.6	-47.2	85.1	-29.6	95.5	-17.6		51	-95.4	-106.6	-107.8	-99.9	-116.2	-94.7
7	65.4	-41.2	82.6	-22.6	92.6	-9.7		52	-91.8	-111.1	-104.5	-105.8	-112.9	-101.2
8	61.6	-35.8	79.0	-15.9	88.6	-2.3		53	-87.9	-115.3	-100.4	-111.3	-108.9	-107.3
9	56.7	-31.4	74.4	-10.0	83.7	4.6		54	-83.3	-118.8	-95.8	-116.3	-104.4	-113.0
10	50.0	-28.5	69.0	-4.6	78.1	10.9		55	-78.3	-121.7	-90.8	-120.7	-99.5	-118.1
11	42.5	-27.0	63.4	0.2	72.0	16.6		56	-73.2	-124.1	-85.3	-124.6	-94.1	-122.8
12	35.0	-26.5	56.9	4.1	65.2	21.4		57	-67.3	-125.2	-79.6	-127.8	-88.4	-126.9
13	27.5	-26.9	49.8	6.7	57.8	25.3		58	-63.4	-127.7	-73.6	-130.4	-82.5	-130.5
14	20.9	-27.3	42.6	8.6	50.1	28.3		59	-59.3	-130.0	-67.4	-132.2	-76.3	-133.4
15	15.4	-27.3	35.3	9.7	42.2	30.4		60	-55.0	-131.7	-62.1	-134.7	-69.9	-135.7
16	10.2	-27.8	28.2	10.2	34.2	31.7		61	-50.5	-132.9	-56.9	-137.2	-63.7	-137.9
17	5.4	-28.2	21.4	10.5	26.5	32.5		62	-46.0	-133.6	-51.4	-138.8	-57.8	-140.4
18	1.1	-28.3	15.0	10.4	19.0	33.0		63	-41.7	-134.3	-45.6	-139.6	-51.8	-142.3
19	-3.0	-28.5	8.7	9.9	11.8	33.0		64	-37.5	-134.6	-40.0	-140.2	-45.6	-143.5
20	-6.8	-28.5	2.8	9.1	4.7	32.7		65	-33.2	-134.5	-34.7	-141.1	-39.5	-144.6
21	-10.5	-28.6	-2.8	8.9	-2.0	32.3		66	-29.1	-134.0	-29.3	-141.5	-33.3	-145.0
22	-14.1	-28.7	-8.2	8.9	-8.5	32.1		67	-25.1	-133.4	-24.0	-141.3	-27.2	-145.4
23	-17.6	-28.8	-13.5	8.7	-14.9	32.1		68	-21.2	-132.8	-18.7	-140.7	-21.1	-145.6
24	-21.1	-28.6	-18.7	8.9	-21.3	31.8		69	-17.5	-132.5	-13.5	-140.1	-15.1	-145.2
25	-24.7	-28.4	-24.0	9.2	-27.6	31.5		70	-13.8	-132.2	-8.4	-139.4	-9.1	-144.5
26	-28.3	-28.2	-29.4	9.0	-34.0	31.1		71	-10.0	-131.8	-3.3	-139.0	-3.2	-143.9
27	-32.0	-28.3	-34.7	8.1	-40.4	30.4		72	-6.3	-131.5	1.9	-138.7	2.9	-143.4
28	-35.7	-28.5	-40.0	7.3	-46.8	29.2		73	-2.4	-131.1	7.3	-138.5	9.3	-143.4
29	-39.6	-28.7	-45.7	6.9	-53.1	27.4		74	1.6	-130.9	13.1	-138.6	16.0	-143.4
30	-43.9	-28.6	-51.7	6.5	-59.4	25.6		75	5.9	-130.7	19.2	-138.9	23.0	-143.2
31	-48.6	-28.2	-57.3	5.0	-66.0	23.9		76	10.6	-130.8	25.8	-138.9	30.4	-143.0
32	-53.4	-28.4	-62.4	2.3	-72.6	21.7		77	15.6	-130.7	32.4	-138.4	37.7	-141.7
33	-58.1	-29.4	-68.7	0.9	-79.0	18.9		78	21.4	-131.0	39.3	-137.3	45.0	-139.8
34	-62.6	-30.8	-74.8	-1.3	-85.1	15.4		79	28.0	-131.5	46.1	-135.6	52.5	-137.5
35	-66.5	-33.4	-80.7	-4.1	-91.0	11.4		80	34.6	-131.0	52.7	-132.9	59.7	-134.1
36	-70.4	-36.0	-86.3	-7.5	-96.5	6.7		81	40.9	-129.5	58.9	-129.4	66.7	-130.2
37	-76.5	-37.4	-91.6	-11.6	-101.5	1.6		82	47.6	-127.5	65.3	-125.6	73.4	-125.5
38	-81.7	-40.0	-96.5	-16.2	-106.0	-4.1		83	53.7	-124.5	70.9	-120.8	79.5	-120.0
39	-86.7	-43.1	-100.9	-21.4	-110.1	-10.1		84	59.4	-120.7	75.9	-115.4	84.9	-113.8
40	-91.3	-46.9	-105.0	-26.9	-113.8	-16.4		85	64.1	-116.1	80.4	-109.4	89.5	-106.9
41	-95.1	-51.4	-108.4	-32.9	-117.0	-23.0		86	67.4	-110.5	84.2	-102.9	93.6	-99.7
42	-98.2	-56.3	-111.3	-39.2	-119.4	-30.0		87	69.4	-104.3	86.7	-96.0	96.9	-92.0
43	-100.7	-61.6	-113.4	-45.8	-121.2	-37.1		88	70.8	-98.1	88.4	-88.7	99.5	-84.0
44	-102.4	-67.2	-114.7	-52.6	-122.5	-44.3		89	71.6	-91.7	89.8	-81.3	101.4	-75.8
45	-103.1	-73.0	-115.3	-59.5	-123.3	-51.7		90	71.6	-85.3	90.1	-73.9	102.5	-67.4

<b>SPIRE</b>	<b>Technical Note</b>						Ref:	SPIRE-RAL-NOT-000993
	Cryostat aperture size requirements including the effects of SPIRE-HERSCHEL misalignments						Issue:	1.00
							Date:	31 October 2001
							Page:	18 of 21

**Table 5-2 (Y,Z) co-ordinates of 90 3-sigma beam boundary points in three selected planes**

point	X = 523		X = 973		X = 1252			point	X = 523		X = 973		X = 1252	
	Y ESA	Z ESA	Y ESA	Z ESA	Y ESA	Z ESA			Y ESA	Z ESA	Y ESA	Z ESA	Y ESA	Z ESA
1	60.7	-77.1	79.7	-67.8	92.1	-61.9		46	-93.3	-77.1	-105.8	-67.8	-113.6	-61.9
2	60.2	-71.3	79.5	-60.9	91.8	-53.8		47	-93.3	-82.1	-105.5	-73.9	-113.1	-68.2
3	59.8	-65.6	78.9	-54.0	91.4	-45.7		48	-92.9	-87.0	-104.6	-79.8	-112.3	-74.4
4	59.5	-59.7	78.4	-47.1	90.5	-37.6		49	-92.0	-91.9	-103.0	-85.6	-110.9	-80.4
5	58.6	-54.0	77.2	-40.1	88.9	-29.6		50	-90.0	-96.6	-100.7	-91.2	-108.9	-86.3
6	57.5	-48.1	75.8	-33.2	86.4	-21.8		51	-87.2	-100.8	-98.3	-96.6	-106.4	-92.0
7	54.6	-43.0	73.4	-26.6	83.6	-14.1		52	-84.1	-104.7	-95.2	-101.6	-103.5	-97.4
8	49.7	-38.9	69.9	-20.4	79.7	-6.9		53	-80.8	-108.3	-91.6	-106.3	-100.1	-102.5
9	42.0	-37.0	65.3	-15.0	74.8	-0.4		54	-76.7	-111.2	-87.5	-110.4	-96.2	-107.2
10	33.8	-36.5	60.1	-10.1	69.2	5.6		55	-72.3	-113.5	-83.0	-114.1	-92.0	-111.5
11	25.5	-37.1	54.5	-5.9	63.0	10.9		56	-67.5	-115.2	-78.2	-117.2	-87.4	-115.3
12	19.0	-37.4	47.7	-3.2	56.0	15.1		57	-62.6	-116.2	-73.1	-119.8	-82.6	-118.7
13	13.6	-37.4	40.7	-1.2	48.5	18.3		58	-59.3	-118.3	-67.8	-121.7	-77.6	-121.7
14	8.4	-38.0	33.6	-0.2	40.6	20.5		59	-56.0	-120.4	-62.6	-123.3	-72.4	-124.2
15	4.1	-38.2	26.6	0.2	32.7	21.8		60	-52.4	-122.0	-58.2	-125.5	-67.1	-126.1
16	0.2	-38.4	20.2	0.5	25.0	22.6		61	-48.7	-123.0	-53.8	-127.6	-61.8	-127.8
17	-3.3	-38.5	14.0	0.3	17.7	23.0		62	-44.8	-123.7	-49.1	-129.0	-56.9	-129.9
18	-6.5	-38.5	8.0	-0.3	10.5	23.0		63	-41.2	-124.2	-44.3	-129.6	-52.1	-131.9
19	-9.6	-38.6	2.4	-1.0	3.7	22.6		64	-37.6	-124.6	-39.5	-130.2	-46.9	-133.0
20	-12.5	-38.6	-2.6	-1.1	-2.8	22.3		65	-33.9	-124.5	-35.0	-131.0	-41.8	-134.0
21	-15.4	-38.7	-7.5	-1.1	-9.0	22.1		66	-30.4	-124.1	-30.5	-131.5	-36.6	-134.8
22	-18.1	-38.8	-12.3	-1.2	-15.0	22.1		67	-27.0	-123.6	-26.0	-131.5	-31.5	-135.1
23	-20.8	-38.7	-17.0	-1.2	-20.9	21.8		68	-23.7	-123.1	-21.5	-131.0	-26.3	-135.4
24	-23.5	-38.5	-21.6	-1.0	-26.7	21.6		69	-20.5	-122.7	-17.1	-130.5	-21.2	-135.6
25	-26.2	-38.3	-26.3	-0.8	-32.5	21.2		70	-17.4	-122.5	-12.8	-129.9	-16.1	-135.3
26	-29.0	-38.2	-31.0	-1.3	-38.3	20.6		71	-14.2	-122.2	-8.4	-129.4	-11.0	-134.6
27	-31.8	-38.3	-35.6	-2.2	-44.1	19.5		72	-11.0	-121.9	-4.0	-129.0	-5.8	-134.1
28	-34.7	-38.4	-40.4	-2.8	-49.7	18.0		73	-7.7	-121.5	0.5	-128.7	-0.5	-133.5
29	-37.7	-38.6	-45.4	-3.1	-55.4	16.3		74	-4.3	-121.2	5.3	-128.6	5.1	-133.3
30	-40.8	-38.8	-50.7	-3.5	-61.2	14.8		75	-0.7	-121.0	10.4	-128.5	11.1	-133.4
31	-44.3	-38.6	-55.4	-5.2	-67.1	13.1		76	3.1	-120.8	15.9	-128.7	17.5	-133.4
32	-48.3	-38.2	-60.0	-7.5	-72.8	10.8		77	7.3	-120.7	22.0	-129.0	24.3	-133.2
33	-52.4	-38.4	-65.5	-8.6	-78.3	7.9		78	12.0	-120.8	28.4	-128.8	31.6	-132.8
34	-56.2	-39.2	-70.9	-10.5	-83.5	4.5		79	17.2	-120.7	34.9	-127.9	38.5	-131.1
35	-59.8	-40.7	-76.1	-13.0	-88.5	0.5		80	23.6	-121.2	41.5	-126.5	45.9	-129.2
36	-62.6	-43.2	-81.0	-16.0	-93.0	-3.9		81	30.7	-121.4	47.8	-124.1	53.0	-126.3
37	-66.1	-45.1	-85.6	-19.6	-97.0	-8.7		82	37.1	-120.1	53.8	-120.9	59.8	-122.7
38	-71.4	-46.3	-89.8	-23.7	-100.6	-13.9		83	43.8	-118.3	59.8	-117.3	66.4	-118.3
39	-76.2	-48.4	-93.6	-28.3	-104.0	-19.3		84	49.7	-115.3	64.9	-112.6	72.3	-113.0
40	-80.7	-51.0	-97.1	-33.2	-106.9	-24.9		85	54.9	-111.4	69.5	-107.3	77.4	-107.0
41	-84.6	-54.4	-100.0	-38.4	-109.2	-30.8		86	58.3	-106.4	73.5	-101.6	81.8	-100.4
42	-87.7	-58.3	-102.4	-44.0	-110.9	-36.9		87	60.0	-100.6	76.5	-95.3	85.6	-93.3
43	-90.2	-62.6	-104.1	-49.8	-112.2	-43.1		88	61.2	-94.8	78.2	-88.5	88.5	-85.8
44	-92.1	-67.3	-105.0	-55.8	-113.0	-49.4		89	61.7	-88.9	79.6	-81.7	90.7	-78.0
45	-93.1	-72.1	-105.4	-61.8	-113.5	-55.6		90	61.2	-82.9	80.2	-74.8	92.2	-70.0

<b>SPIRE</b>	<b>Technical Note</b>	Ref:	SPIRE-RAL-NOT-000993
	Cryostat aperture size requirements including the effects of SPIRE-HERSCHEL misalignments	Issue:	1.00
		Date:	31 October 2001
		Page:	19 of 21

## 6. IMPLICATIONS FOR THE SPIRE-HERSCHEL ALIGNMENT BUDGET

The clearance boundaries sought within the cryostat/primary mirror space by the SPIRE instrument are predicated on the RSSQ pupil shear not exceeding 11.2 mm. This figure is obtained by summing in quadrature the contributions of 9.2 mm from the telescope to SPIRE interface and 6.3 mm from the SPIRE instrument alone (justified because their sources are statistically independent and random). The modelling has proceeded by then modelling the system as if the whole 11.2 mm is allotted to the telescope to SPIRE misalignments. Values for the amplitude multiples (N,M) permitted for the individual axis displacements and tilts were then derived using the modelling results from RD2. These derived values are ‘effective’ values in the sense that they are in general bigger than the ‘real’ values should be, since the ‘real’ axis displacements and tilts must only account for the telescope to SPIRE misalignment contribution of 9.2 mm. Therefore, we here determine the ‘real’ displacement and tilt amplitudes that are permitted in order to keep the 3-sigma telescope to SPIRE misalignment equal to 9.2 mm. Figure (6-1) shows the solution of equation (4-1) for  $RSSQ(N,M,3*\sigma) = 9.2$  and table (6-1) shows the details of the plotted values.

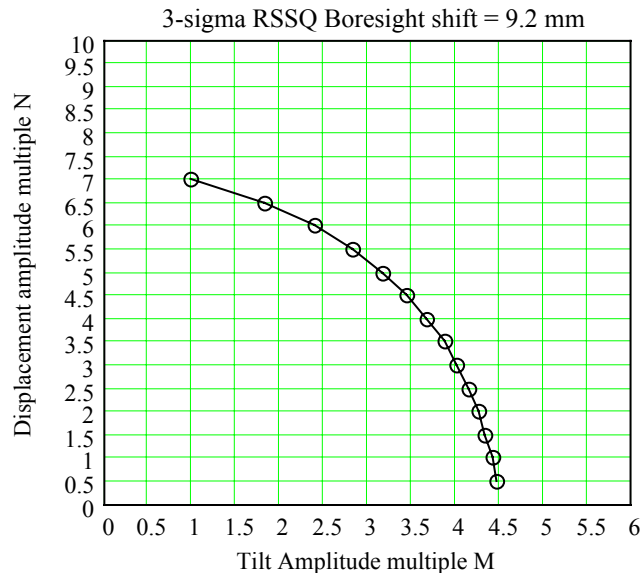


**Figure 6-1 (N,M) solutions to  $RSSQ(N,M,3.0*\sigma,\theta)=9.2$**

N	M	$\theta$
0.5	4.461	6.395
1.0	4.404	12.79
1.5	4.333	19.09
2.0	4.246	25.22
2.5	4.133	31.17
3.0	4.009	36.81
3.5	3.859	42.21
4.0	3.668	47.48
4.5	3.436	52.64
5.0	3.155	57.75
5.5	2.814	62.9
6.0	2.39	68.28
6.5	1.823	74.34
7	0.9644	82.16

**Table 6-1 (N,M, $\theta$ ) solutions to  $RSSQ(N,M,3.0*\sigma,\theta)=9.2$**

<b>SPIRE</b>	<b>Technical Note</b>	Ref:	SPIRE-RAL-NOT-000993
	Cryostat aperture size requirements including the effects of SPIRE-HERSCHEL misalignments	Issue:	1.00
		Date:	31 October 2001
		Page:	20 of 21

Any pair of (N,M) values that fall on the curve shown in figure (6-1) can be selected and the 3-sigma RSSQ value resulting from SPIRE-HERSCHEL misalignments should equal 9.2 mm. The data should be compared to that shown in figure (4-7) and table (4-4), which apply to the case where the 3-sigma RSSQ total = 11.2 mm. In the latter case, an arbitrary choice (N,M)=(6,3.89) was made, which equates to 3 mm displacement per axis and 3.89 arc minutes tilt per axis. In the present case, in order to keep a very similar choice, M=3.86, for the tilt multiple, we must select a smaller value, N=3.5, for the displacement multiple (1.75 mm displacement per axis). Alternatively, in order to keep an identical choice, N=6.0, for the displacement multiple, we must now select a smaller value, M= 2.39, for the tilt multiple (2.39 arc minutes per axis).

In summary, the applicability of the clearance boundaries detailed in the foregoing text depend on the SPIRE-HERSCHEL misalignments being constrained to fixed bands, as illustrated in figures (4-3) and (4-4), and the pair of multiples (N,M) of the basic units (0.5 mm, 1 arc minute) defining the bands must be selected from the curve drawn in figure (6-1) or interpolated from table (6-1). If, in practice, HERSCHEL alignment is shown to be able to achieve an accuracy such that the limits of its misalignments with SPIRE can be characterised by a number pair (N,M) that fall **below** the curve shown, then the clearance boundaries required by SPIRE could be reduced in size, depending on the improvement in the alignment accuracy achievable.

## 7. A NOTE ON CO-ORDINATE REFERENCE FRAMES USED

Two different co-ordinate systems are used in this analysis. They are indicated in figure 7-1. When the location of a plane normal to the telescope axis is specified, it may be given a Z-value, indicating that the first co-ordinate system is being used. RD1 uses this system, which is naturally derived from the CODEV model used to generate the original ray data, so the figures taken from that note use a Z-value to locate the sectional plane. Points in these sectional planes are located using X- and Y-co-ordinates.

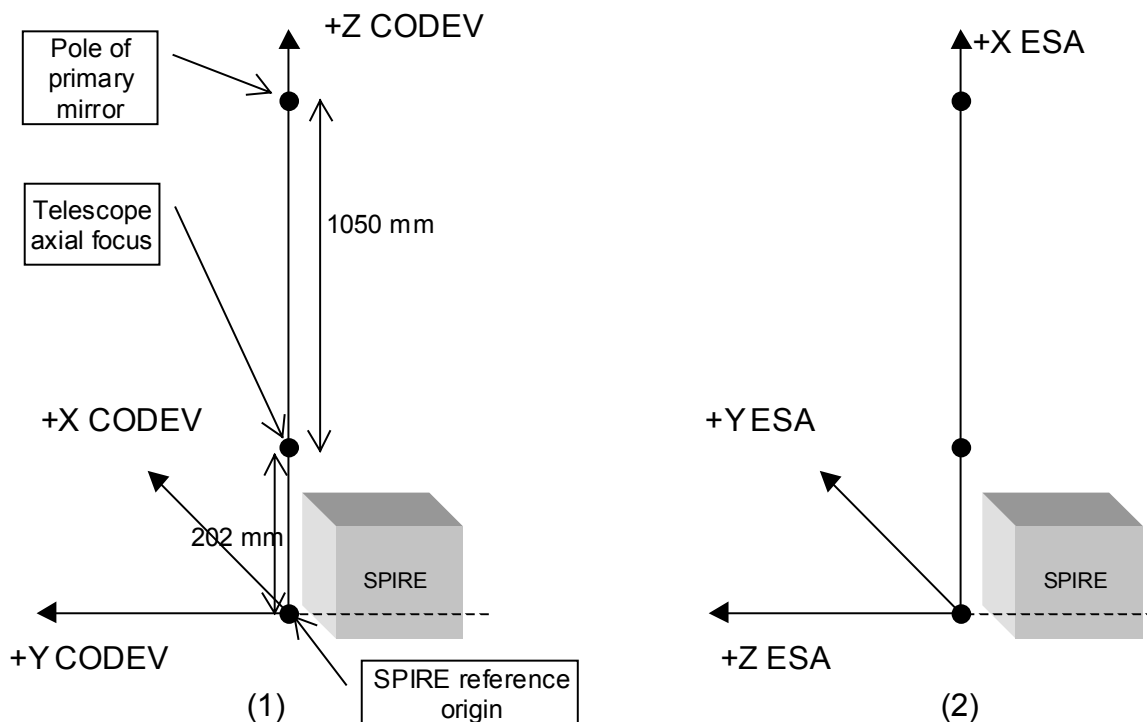


Figure 7-1 Reference co-ordinate systems used.

<b>SPIRE</b>	<b>Technical Note</b>	<b>Ref:</b>	SPIRE-RAL-NOT-000993
	<b>Cryostat aperture size requirements including the effects of SPIRE-HERSCHEL misalignments</b>	<b>Issue:</b>	1.00
		<b>Date:</b>	31 October 2001
		<b>Page:</b>	21 of 21

For consistency with the co-ordinate system adopted within the mechanical design CAD platform used by SPIRE, the sectional plane data are now given in the ESA-oriented reference frame, which is the second one shown. In this frame, a plane normal to the telescope axis is given an X-value. The points in this plane are then located using Y- and Z-co-ordinates. These are the co-ordinates used in tables 5-1 and 5-2.

Both systems locate their origin of co-ordinates at the same point, which is on the telescope axis 202 mm below the telescope axial focus, which itself is designed to be located 1050 mm below the pole of the primary mirror.

## 8. CONCLUSIONS AND RECOMMENDATIONS

1. When considering the location of SPIRE on the HOB and the location of the HOB in the cryostat, it is assumed that the limits on the deviation of the location from the optimum can be expressed as being between + and  $-0.5 \cdot N$  mm per axis and the limits on the deviation of the orientation from optimum can be expressed as being between + and  $-M$  arc minutes, per axis.
2. In order to be >99% sure that the RSSQ pupil shear contribution due to these misalignments be < 9.2 mm, then the point (N, M) must lie on or below the curve shown in figure 6-1.
3. If the point (N,M) lies on the curve, then the 3-sigma boundary curves at the three chosen sectional planes will be very close to those shown in figures 5-1, 5-2 and 5-3 and listed in table 5-2. In this case, SPIRE requires that cryostat and primary mirror structure remain outside the clearance boundaries shown in the same figures and listed in table 5-1, assuming that a minimum 10 mm clearance is adequate (TBC).
4. If the HERSCHEL alignment uncertainties, as parameterised by the number pair (N, M), are or become such that the point (N, M) lies BELOW the curve, then the 3-sigma boundary curves and the clearance curves sought by SPIRE can be REDUCED in size commensurately. The amount of the reduction can be derived by re-running the simulation with the actual values for (N, M).
5. If the HERSCHEL alignment uncertainties, as parameterised by the number pair (N, M), are or become such that the point (N, M) lies ABOVE the curve, then the 3-sigma boundary curves and the clearance curves sought by SPIRE must be INCREASED in size commensurately. The amount of the INCREASE can be derived by re-running the simulation with the actual values for (N, M).
6. SPIRE requires that a clearance boundary be generated by adding a minimum clearance of 10 mm (TBC) to the 3-sigma composite beam boundary computed using the particular (N, M) pair that applies.
7. Whatever the size computed for the clearance boundary in whatever plane, SPIRE requires that the edges of cryostat apertures and primary mirror hole structure remain on or outside the clearance boundary computed in that plane.